

Concrete Constitutive Model, Calibration and Applications

Javier Rodríguez, Francisco Martínez, and Joaquín Martí

Principia, Velázquez 94, 28006 Madrid, Spain

Abstract: A methodology has been developed for characterising the mechanical behaviour of concrete, based on the damaged plasticity model, enriched with a user subroutine (V)USDFLD in order to capture better the ductility of the material under moderate confining pressures. The model has been applied in the context of the international benchmark IRIS_2012, organised by the OECD/NEA/CSNI Nuclear Energy Agency, dealing with impacts of rigid and deformable missiles against reinforced concrete targets.

A slightly modified version of the concrete damaged plasticity model was used to represent the concrete. The simulation results matched very well the observations made during the actual tests. Particularly successful predictions involved the energy spent by the rigid missile in perforating the target, the crushed length of the deformable missile, the crushed and cracked areas of the concrete target, and the values of the strains recorded at a number of locations in the concrete slab.

Keywords: Concrete, Impact, Perforation

1. Introduction

The present paper deals with the ability of numerical simulation to model the effects of impacts on reinforced concrete slabs. The need to analyse this situation arises in many fields, but the specific orientation here is the requirement imposed on nuclear facilities of studying the effects of various types of postulated impacts.

In the analysis of these impacts the missiles are conveniently classified into rigid and deformable, depending on their deformability in comparison with the target. A turbine rotor sector can be considered an example of the former, while an aircraft crash is a typical instance of the latter.

The ability to simulate this type of problems is evaluated here by comparing the numerical results obtained in calculations with the observations produced in physical tests. The reported activities were carried out in the context of an international benchmark exercise, named IRIS_2012, organised by the OECD/NEA/CSNI Nuclear Energy Agency.

The impact tests performed, which included both rigid and deformable missiles, were conducted at the Technical Research Center of Finland (VTT, 2010). A number of characterisation tests (such as uniaxial compression tests, Brazilian tests, and triaxial compression tests at various confining pressures) were also provided in order to describe the behaviour of the concrete and to allow determining the parameters of the constitutive model selected by the benchmark participants.

The rest of the paper describes the approach followed by Principia for modelling the impact tests and contributing to the international benchmark.

2. Concrete model and properties

2.1 Concrete damaged plasticity

When modelling reinforced concrete, one could adopt a single material model to represent both the mass concrete and the steel reinforcement; this is a reasonable alternative when dealing with moderate loads, far from the ultimate capacity of the materials, with mainly elastic responses being triggered. At a greater level of demands, with the concrete cracking and the steel yielding, this is no longer practical and the two materials must be modelled individually.

For those more demanding situations, Abaqus (SIMULIA, 2012a) has a number of models of varying complexity, suitable for modelling the behaviour of mass concrete, with the reinforcing bars embedded in the concrete. Out of those the concrete damaged plasticity model is the one adopted for the present calculations.

This model provides a general capability for analysis of concrete structures under monotonic, cyclic, and/or dynamic loading. It includes a scalar (isotropic) damage model with tensile cracking and compressive crushing modes. The model accounts for the stiffness degradation mechanisms associated with the irreversible damage that occurs during the fracturing process.

The model actually used in the simulations is not exactly that described in SIMULIA (2012b) as the damaged plasticity model since, as explained later, Principia modified it slightly to achieve a better representation of the response under moderate confinement.

2.2 Calibration of the concrete model

A number of tests were provided for calibration of the parameters of the concrete model selected by the benchmark participants (IRSN, 2012). Also, some parameters were given directly: a density of 2273 kg/m³, a Young's modulus of 29.7 GPa, and a Poisson's ratio of 0.223.

Figure 1 presents the results of unconfined and triaxial tests performed at various confining pressures: 15.5, 26, 47 and 100 MPa, with greater confining pressures leading to a higher peak stress and less post-peak softening. The strength characteristics can also be observed using Mohr circles (Figure 2), which indicate that the resulting friction angle is $\phi = 30.8^\circ$.

The concrete damaged plasticity model uses a non-associated flow potential. The flow potential G used for this model is the Drucker-Prager hyperbolic function, which neglecting damage can be approximately expressed as:

$$G = q - p \tan \psi \quad (1)$$

where q is the von Mises stress, p is the pressure invariant of the stress tensor, and ψ is the dilation angle.

For triaxial tests the dilation angle can be obtained from:

$$\tan \Psi = \frac{3}{2} \frac{2\nu_p - 1}{1 + \nu_p} \quad (2)$$

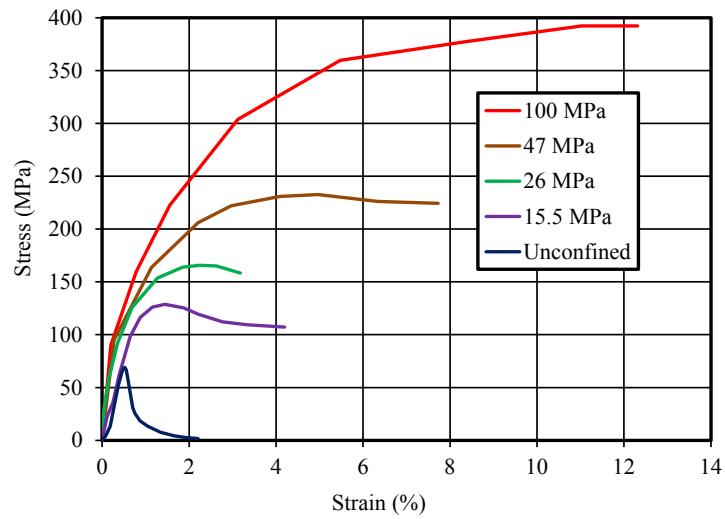


Figure 1. Uniaxial unconfined and tri-axial tests

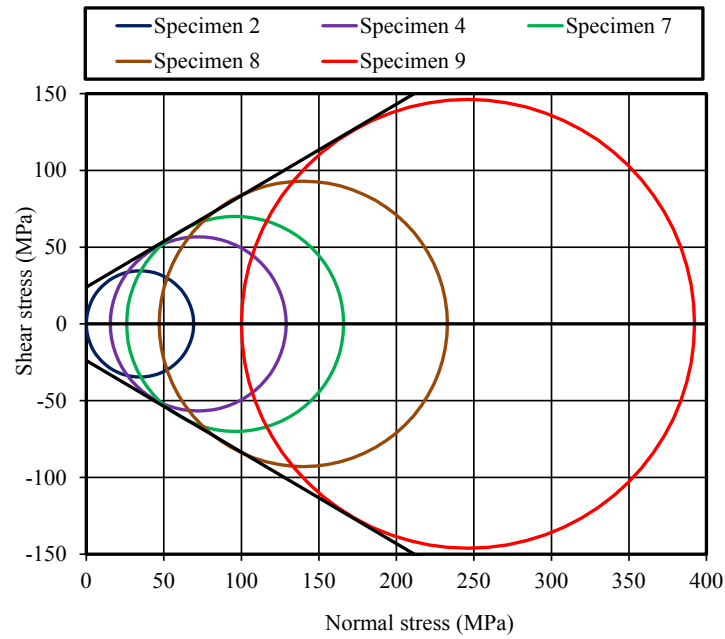


Figure 2. Concrete tests in Mohr's representation

where ν_p is the apparent Poisson's ratio for yielding. Using the data from the triaxial tests at various confining pressures, the above leads to an average dilation angle of 30° .

For high confining pressures the yield condition for undamaged concrete tends to be defined by:

$$F = q - 3\alpha p + \gamma \sigma_{\max} \quad (3)$$

where α is related to the ratio of the biaxial stress, σ_b , to the uniaxial stress, σ_c , through

$$\frac{\sigma_b}{\sigma_c} = \frac{1 - \alpha}{1 - 2\alpha} \quad (4)$$

σ_{\max} is the maximum principal stress (compression being negative), and γ is defined by

$$\gamma = \frac{3(1 - K_c)}{2K_c - 1} \quad (5)$$

where K_c is a material parameter between 0.5 and 1.0; a value of 0.75 is assumed here.

It can also be shown that α can be expressed as a function of the friction angle φ :

$$\alpha = \frac{3K_c + K_c \sin \varphi + \sin \varphi - 3}{6K_c + \sin \varphi - 2K_c \sin \varphi - 3} \quad (6)$$

This leads to $\alpha = 0.117$ and the ratio of the biaxial to the uniaxial compressive stresses is 1.15. On the other hand, going back to equation (3), if the effects of the effective compressive cohesion stress σ_c are not neglected, the actual yield condition can be expressed as:

$$F = q - 3\alpha p + \gamma \sigma_{\max} + \sigma_c(\varepsilon_p) \quad (7)$$

Using the above equation ($F = 0$), Figure 3 presents the compressive cohesion stress that results for the five reference tests supplied. For a good reproduction of the data, the compressive cohesion stress was taken to be a function not only of the equivalent plastic strain but also of the maximum principal stress. This is accomplished by a (V)USDFLD Abaqus user subroutine.

The Brazilian tests indicated that the tensile strength of the concrete is about 4 MPa. No fracture energy was provided, but it is typically 40 N/m for a concrete with 20 MPa compressive strength and 120 N/m for one with 40 MPa. Extrapolating to 69 MPa, the fracture energy would be 228 N/m, which is the value adopted here; however this parameter though has relatively little influence on the results produced here. Finally, strain rate effects did not appear to be very significant and were disregarded.

Having determined all the parameters of the concrete constitutive model, the various calibration tests were reproduced to ensure consistency. Figure 4 plots the results of the simulations (solid lines) together with the experimental data (dots). Although some deviations appear at the higher confining pressures, this constitutive representation was considered sufficient and was adopted for simulating the effects of the punching and bending tests.

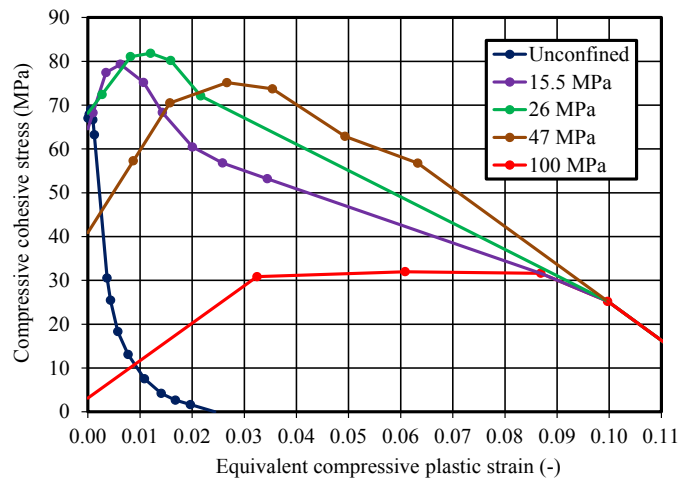


Figure 3. Compressive cohesion stress

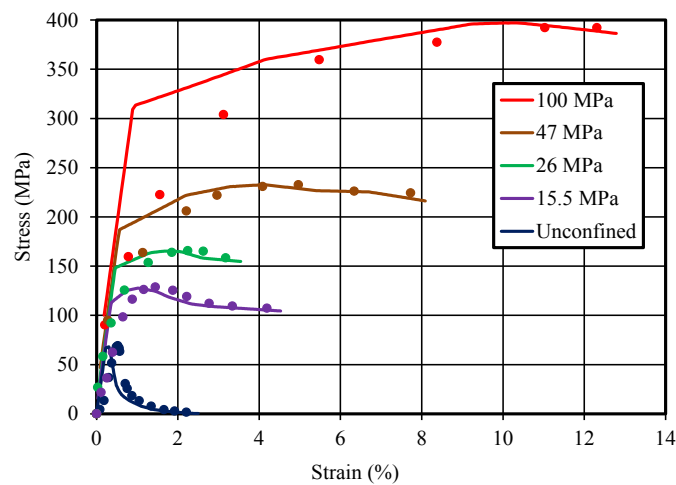


Figure 4. Comparison between tests and concrete material model

3. The bending test

3.1 Description

Only the more salient points of the bending test will be described here; interested readers can find further details in VTT (2010). A reinforced concrete slab, spanning 2 m by 2 m and with a thickness of 150 mm (Figure 5), is held in a very rigid supporting frame. The longitudinal reinforcement provided in the slab is $5 \text{ cm}^2/\text{m}$ in each direction, made of 6 mm diameter bars at 55 mm spacing, and the quantity of transverse rebars was $50 \text{ cm}^2/\text{m}^2$. The outer edge of the slab is strengthened with C shaped steel elements.

A stainless steel missile with a mass of 50 kg is then thrown against the slab with a nominal velocity of 110 m/s; a drawing of the missile appears in Figure 6. The missile is very deformable and can be expected to buckle extensively upon impact, leading to a sustained load on the wall that corresponds to the collapse load of the missile.

Two tests of this type were conducted, in which the actual velocities were 110.15 and 111.56 m/s; the present simulation deals with the first one. Many types of data were acquired during the tests.

3.2 Finite element model

Because of symmetry only a quarter model was built, with the geometry shown in Figure 7a. Displacements were prevented along the support line in a direction perpendicular to the slab. The reinforcing bars were explicitly included in the model with beam elements embedded in the concrete solid elements (Figure 7b).

Based on that geometry an Abaqus/Explicit finite element model was generated for the slab, the reinforcing bars and the missile; the softness of the latter would have allowed representing it by an estimated load history, but it was decided to model its actual deformations. Ten brick elements were in the thickness were used. The concrete was endowed with the constitutive behaviour of the previous section, except at the edge where it is strengthened with steel elements and assumed to remain elastic.

For the reinforcing steel, an elastoplastic model was used, based on the properties supplied by the organisers, with a yield stress of 661.7 MPa. The stainless steel of the missile was considered to be elastoplastic and with the properties provided: the 0.5 proof yield stress is 350.7 MPa, the tensile strength is 633 MPa, and the ultimate elongation is 45.4%.

In the course of the impact a number of contacts take place between the various materials; a coefficient of friction of 0.3 was used at all interfaces. The general contact algorithm is defined at all external surfaces.

3.3 Results

A first verification is afforded by comparing the calculated and observed deformations of the missile. As shown in Figure 8, the comparison is very satisfactory: starting from an initial missile length of 2111 mm, the calculations indicate that this length would reduce to 1052 mm, against the 1130-1150 mm observed in the tests. It was hence concluded that the simulation of the missile behaviour produces a realistic representation of the loading applied on the slab.

The crushing strains produced by the impact in the concrete wall are shown in Figure 9; they concentrate in the front face of the slab and are practically inexistent at the back. Figure 10 displays the zones that have undergone some cracking as a result of the impact. The missile is fully arrested in a little under 20 ms from the onset of impact.

The effects on the reinforcement can be visualised in Figure 10 (right): yielding is essentially restricted to bars located in the back face of the wall and at or near the impact region.

The calculated and recorded displacements at the centre of the wall appear in Figure 11. The match is very good up to the peak; the subsequent differences arise because, as already mentioned, the concrete model does not return the load path to the origin. Those differences do not constitute a significant drawback when modelling a primarily impulsive event.

As a conclusion, it can be stated that the constitutive model adopted for the concrete and the material parameters determined from the tests on laboratory samples allowed performing a very realistic simulation of the bending test and its effects on the target slab.

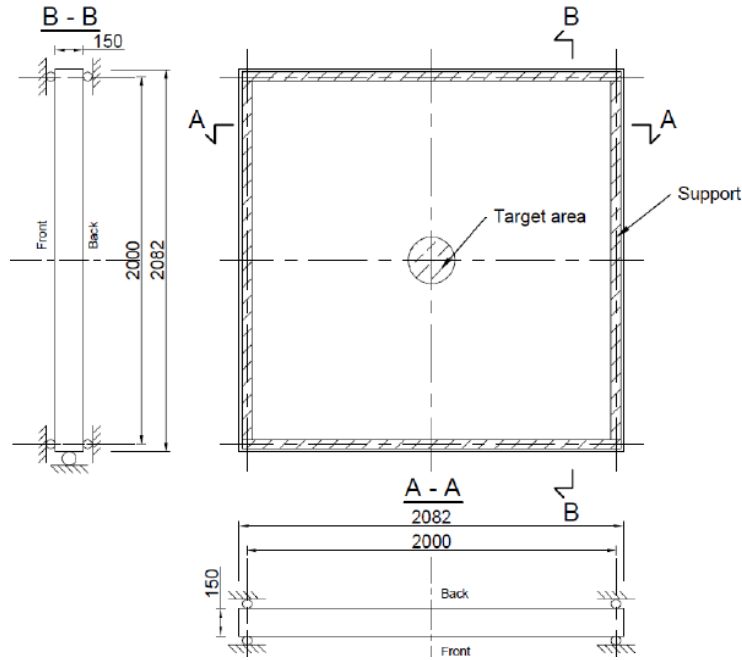


Figure 5. Geometry and supports of the wall in the bending test

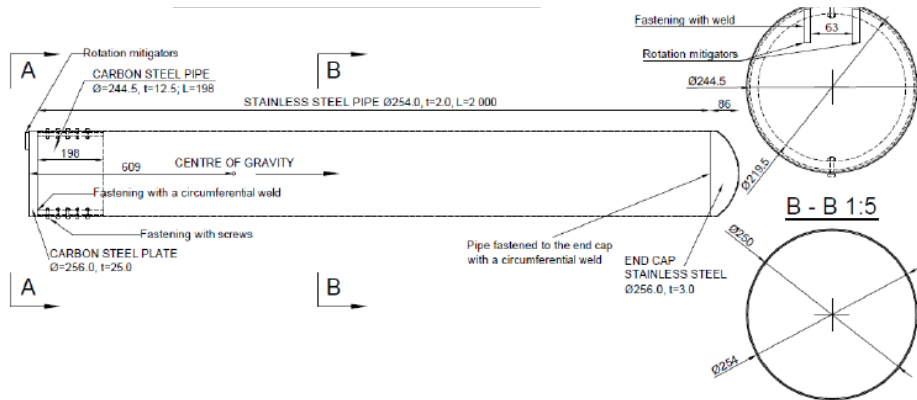


Figure 6. Drawing of the deformable stainless steel missile

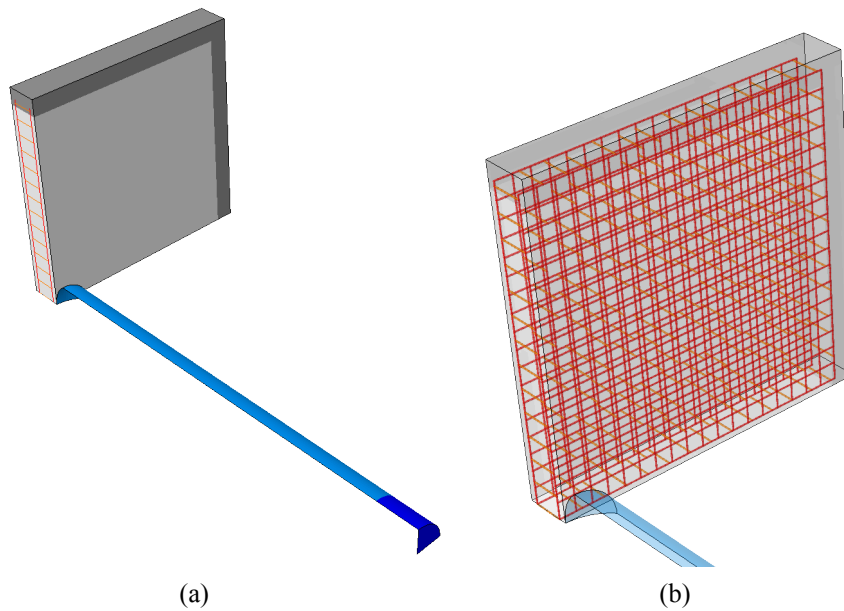
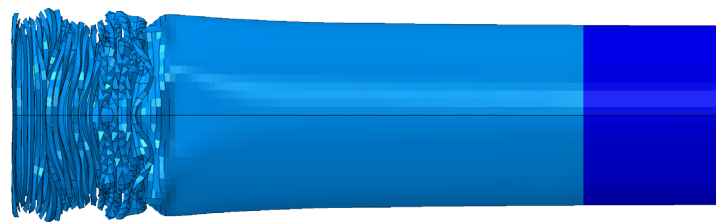
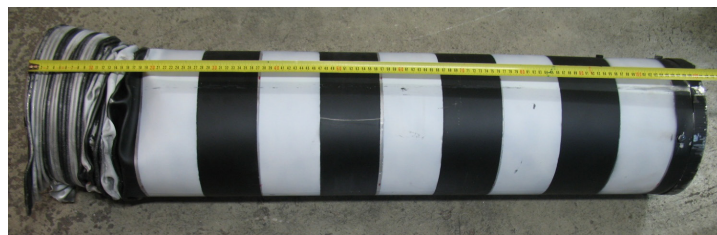


Figure 7. Geometry and rebars of the model for the bending test



Model



Test

Figure 8. Missile after the bending impact test

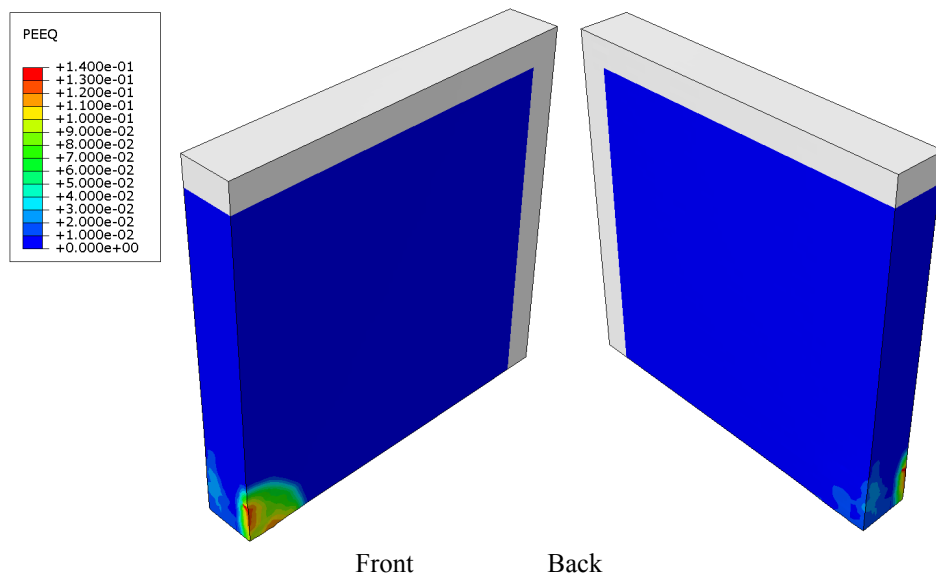


Figure 9. Crushing strains after the bending test (-)

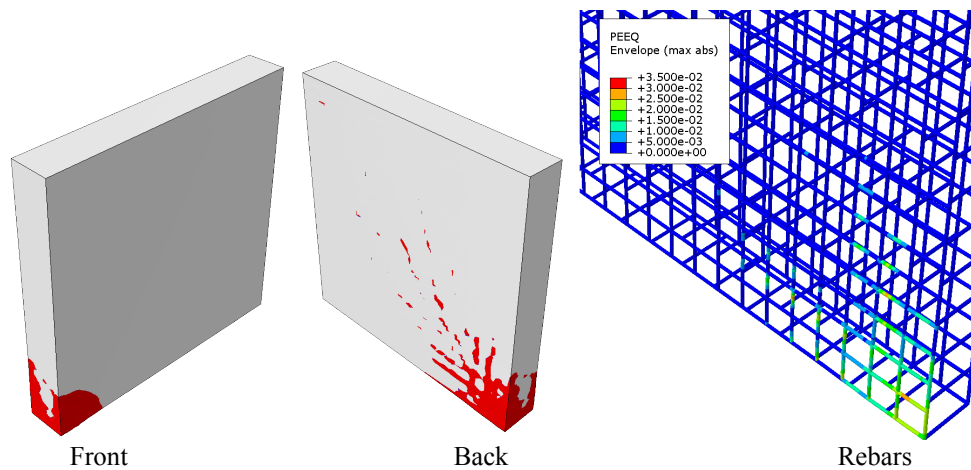


Figure 10. Zones with cracks an plastic strains after the bending test

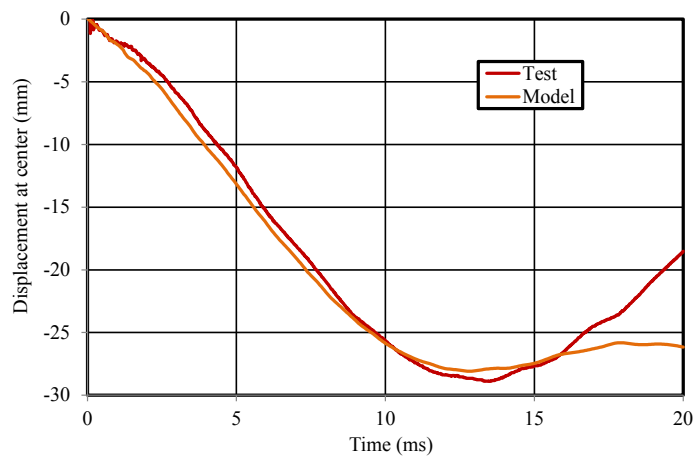


Figure 11. Centre displacement during the bending impact test

4. The punching test

4.1 Description

Again, only the more significant aspects will be described here, additional details are provided by VTT (2010). The missile differs considerably from that of the bending test, as it is now intended to be much less deformable than the target. The steel tube is thicker and filled with concrete (Figure 12); the nominal mass of the missile was 50 kg, but its actual mass of 47.4 kg is the one used in the calculation. Three tests were conducted with similar missile velocities; in the one simulated here the measured velocity was 136 m/s.

As in the bending test, the slab spans 2 m by 2 m and is held in the same supporting frame, but the wall thickness is now 250 mm. Only longitudinal reinforcement was provided, no transverse reinforcement was present; the quantity was $8.7 \text{ cm}^2/\text{m}$ in each direction, consisting of 10 mm diameter bars at 90 mm spacing. The average yield stress of the steel was 540 MPa and its tensile strength was 605.3 MPa with an ultimate elongation of 18.7%.

4.2 Finite element model

The quarter symmetry was again incorporated and the geometry of the model appears in Figure 13a. The reinforcing bars are included in the model, as seen in Figure 13b. Based on that geometry a finite element model was generated without introducing any special considerations with respect to the bending test model; a detail of the mesh can be seen in Figure 13c.

To avoid excessive and unrealistic distortions, elements are removed from the mesh when their equivalent plastic strain reaches 0.3; their stiffness contribution is already negligible after about 0.13, but premature deletion should be avoided. Deletion is implemented by defining a state variable which is updated in the VUSDFLD user subroutine. For the reinforcing steel, an elastoplastic model was used with the properties supplied by the organisers. The coefficient of

friction was again taken to be 0.3 at all contact interfaces. In this case, apart from the contact between external surfaces, interactions with internal were also included.

Although the deformability of the missile is small compared to that of the target, a finite element model of the missile was also constructed. This influences only the details of the momentum transfer in the initial phase of the impact.

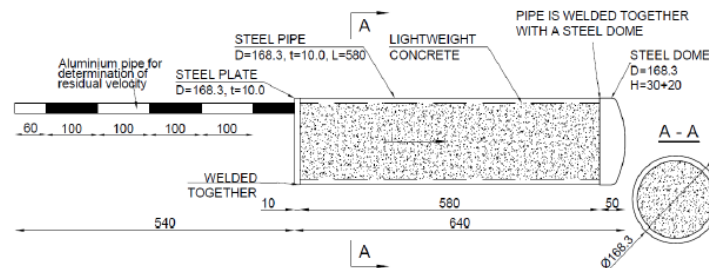


Figure 12. Drawing of the hard missile

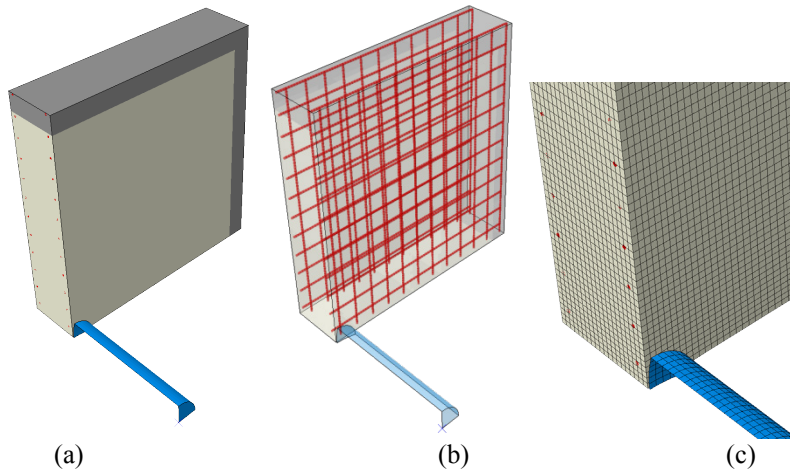


Figure 13. Geometry, rebars and mesh of the punching model

4.3 Results

The missile clearly perforates the slab. The results of the simulations 10 ms after the onset of impact, is presented in Figure 14; the large displacements that appear in the back face of a seemingly solid wall should not be taken literally, they simply evince the delay in deleting concrete elements when the reinforcement at the back face is losing its concrete cover.

An outer view of the distribution of crushing strains appears in Figure 15. The outer concrete cover is being lost in some areas.

The calculated and observed cracked zones can be visually compared in Figure 16. Although of a qualitative nature, the comparison indicates that the cracking configurations and extents are very realistic, in both the front and back faces of the slab.

The effects on the reinforcement are shown in Figure 17. The yielding of rebars is fairly localised in the front face and less so in the back face; large deformations and failure of rebars occurs as the missile perforates the concrete slab.

The kinetic energy of the emerging missile affords a very relevant comparison between the simulation and test results. The energy dissipated in the test while perforating the concrete wall was 408 kJ, while that determined by the calculations was 358 kJ. The approximation is considered very reasonable, particularly when taking into account that the materials have been assumed to go suddenly to zero stress at the end of the stress-strain curves provided as reference; any elongation of those curves, or a more gradual decrease towards zero, would lead to a somewhat greater dissipation of energy during the perforation process.

Additionally, a conversion from finite element to smoothed particle hydrodynamic methods (SPH) has been activated. This is a new technique supported in Abaqus version 6.12. SPH is a fully Lagrangian modeling scheme permitting the discretization of a prescribed set of continuum equations by interpolating the properties directly at a discrete set of points distributed over the solution domain without the need to define a spatial mesh. In our analysis each conventional brick element is automatically converted to eight SPH particles when the equivalent plastic strain reaches 0.2. The resulting deformed configuration with contours of equivalent plastic strains at 10 ms is shown in Figure 18. The energy of the missile dissipated during perforation is now 394 kJ.

The peak contact force between the missile and the slab obtained during the simulation was 20.78 MN. This value is expected to be greater than the actual one because the impactor was assumed to be rigid in the simulation. To evaluate the influence of this simplification a new model was constructed using a deformable missile. The deformed mesh and crushing strains are presented in Figure 19. Also, the kinetic energy of the missile is provided in Figure 20. It can be concluded that the assumption of rigid missile does influence the time evolution of the contact force, but the final outcome remains essentially unaffected; this is because the problem is controlled by the total impulse transferred, which is similar in both cases, only the rate of transfer is affected.

Based on the foregoing, the concrete model adopted and the calibrated material parameters allowed performing a very realistic simulation of the punching test and its effects on the slab. Also, the conversion to SPH after the initial phases led to an improved prediction of the response.

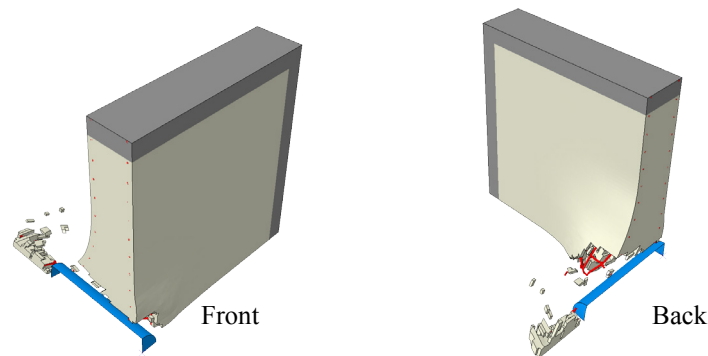


Figure 14. Deformation after 10 ms during punching

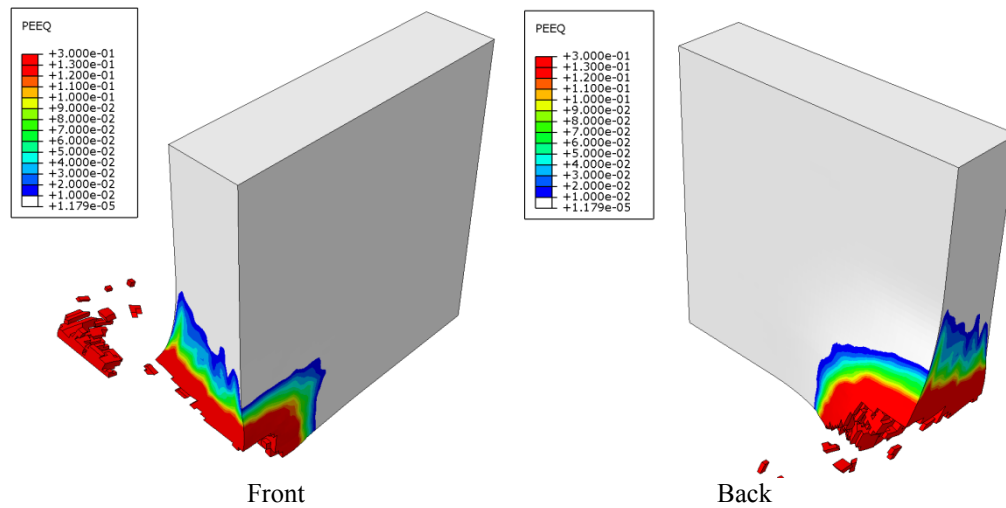


Figure 15. Crushing strains after the punching test

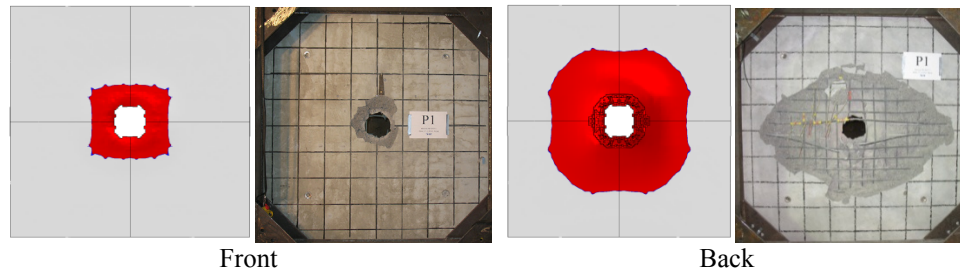


Figure 16. Crack zones after the punching test

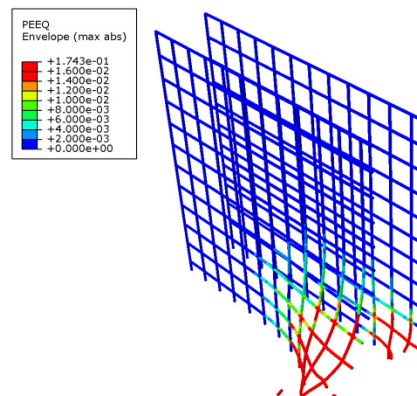


Figure 17. Plastic strains in rebars after the punching test (-)

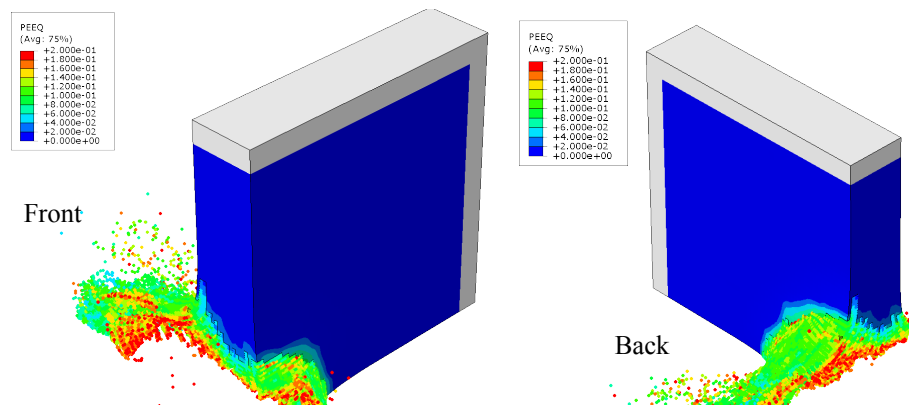


Figure 18. Crushing strains during the punching test with SPH conversion

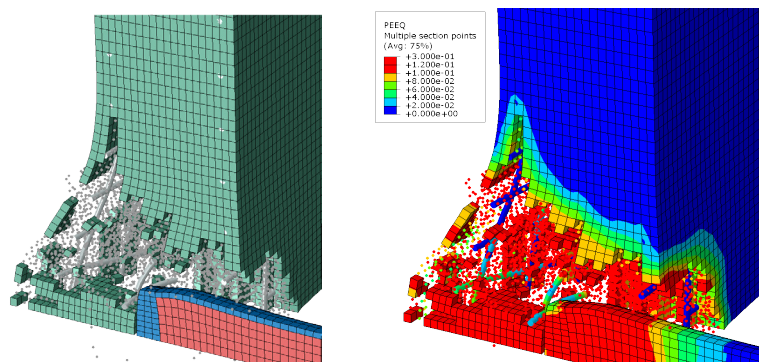


Figure 19. Deform. and crushing strains during punching with a deformable missile

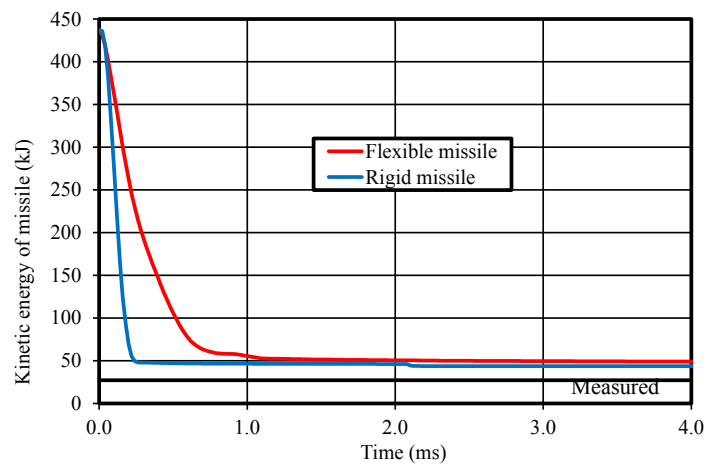


Figure 20. Comparison of missile energies with rigid and deformable missiles

5. Conclusions

A number of activities have been carried out within the framework of the IRIS_2012 international benchmark, dealing with the simulation of impacts on reinforced concrete slabs. The concrete damaged plasticity model was slightly modified to improve reproduction of the characterisation tests, used to calibrate the parameters of the model. Having done this, the two benchmark tests were simulated: a soft missile impact (named the bending test) and a rigid one (punching test). As a result of this work, the following conclusions can be offered:

- The damaged plasticity model available in Abaqus has proved to be very adequate for describing the concrete behaviour observed in the characterisation tests, the bending test, and the punching test.
- The modification introduced by Principia in the damaged plasticity model, which consisted in making the compressive cohesion stress to depend also on the maximum signed principal stress, has also been shown to be successful.
- The model used is considered to be particularly suitable for primarily impulsive situations, such as contemplated in IRIS_2012, in which the concrete is subjected to an essentially monotonic loading path and the subsequent unloading is less important.
- The minor differences observed between the calculated and test results, such as wall centre displacements upon unloading in the bending test, can be traced to known features of the model, which could be improved if warranted.
- The conversion to smoothed particle hydrodynamics (SPH), activated as an alternative strategy for rerunning the punching test, improved the prediction of energy dissipation.

6. References

1. SIMULIA “Abaqus Analysis User’s Manual”, Version 6.12, Dassault Systèmes Simulia Corp., Providence, RI, 2012a.
2. SIMULIA “Abaqus Theory Manual”, Version 6.12, Dassault Systèmes Simulia Corp., Providence, RI, 2012b.
3. CSNI – Committee on the Safety of Nuclear Installations, “Activity Proposal Sheet. Improving Robustness Assessment of Structures Impacted by Missiles (IRIS_2010)”, February, 2012.
4. IRSN Institut de Radioprotection et Sûreté Nucléaire, “IRIS_2012. Uniaxial and Tri-Axial Concrete Test”, February, 2012.
5. VTT – Technical Research Center of Finland, “Experimental Tests for Bending and Punching Behaviour of Reinforced Concrete Walls under Impact Loading”, August, 2010.